

Sub-10 nm Resolution Patterning of Pockets for Enzyme Immobilization with Independent Density and Quasi-3D Topography Control

Xiangyu Liu,[†] Mohit Kumar,[‡] Annalisa Calo,[†] Edoardo Albisetti,^{†,§} Xiaorui Zheng,[†] Kylie B. Manning,^{||} Elizabeth Elacqua,^{||,⊥} Marcus Weck,^{||} Rein V. Ulijn,^{*,‡} and Elisa Riedo^{*,†}

[†]Tandon School of Engineering, New York University, Brooklyn, New York 11201, United States

[‡]Advanced Science Research Center (ASRC), CUNY Graduate Center, New York, New York 10031, United States

[§]Dipartimento di Fisica, Politecnico di Milano, Milano, 20133, Italy

^{||}Department of Chemistry, New York University, New York, New York 10003, United States

[⊥]Department of Chemistry, The Pennsylvania State University, University Park, Pennsylvania 16802, United States

Supporting Information

ABSTRACT: The ability to precisely control the localization of enzymes on a surface is critical for several applications including biosensing, bionanoreactors, and single molecule studies. Despite recent advances, fabrication of enzyme patterns with resolution at the single enzyme level is limited by the lack of lithography methods that combine high resolution, compatibility with soft, polymeric structures, ease of fabrication, and high throughput. Here, a method to generate enzyme nanopatterns (using thermolysin as a model system) on a polymer surface is demonstrated using thermochemical scanning probe lithography (tc-SPL). Electrostatic immobilization of negatively charged sulfonated enzymes occurs selectively at positively charged amine nanopatterns produced by thermal deprotection of amines along the side-chain of a methacrylate-based copolymer film via tc-SPL. This process occurs simultaneously with local thermal quasi-3D topographical patterning of the same polymer, offering lateral sub-10 nm resolution, and vertical 1 nm resolution, as well as high throughput ($5.2 \times 10^4 \mu\text{m}^2/\text{h}$). The obtained single-enzyme resolution patterns are characterized by atomic force microscopy (AFM) and fluorescence microscopy. The enzyme density, the surface passivation, and the quasi-3D arbitrary geometry of these patterned pockets are directly controlled during the tc-SPL process in a single step without the need of markers or masks. Other unique features of this patterning approach include the combined single-enzyme resolution over mm^2 areas and the possibility of fabricating enzymes nanogradients.

KEYWORDS: Scanning Probe Lithography, Enzyme Nanopatterning, Biointerface, Bionanotechnology, Nanofabrication, Thermochemical Nanolithography



1. INTRODUCTION

Enzymes can efficiently promote biochemical reactions with great specificity in aqueous environments, and have broad applications as biocatalysts in the food industry and in biomedicine. The ability to immobilize and pattern enzymes on a solid surface with a predefined spatial configuration is relevant for many bionanotechnological and biological applications, such as biosensing, bionanoreactors, enzyme-assisted lithography, and cell biology studies.^{1–8} As the size of the bionanotechnological devices continues to scale down, the capability of fabricating enzyme patterns at the nanometer scale is crucial. Highly defined enzyme patterns at this length scale can significantly benefit the fabrication of biosensors with densely packed arrays for highly sensitive and high-throughput detection.^{1,9,10} Due to the catalytic properties of enzymes,

enzyme nanopatterns can also be implemented to grow inorganic materials as device building blocks or to locally degrade macromolecular films, generating templates for the subsequent patterning of miniature electrical circuits.^{2,9,11} Furthermore, quasi-3D patterning on soft polymer surfaces with single enzyme resolution ($<10 \text{ nm}$) allows a more precise engineering of the enzymes' microenvironment, which can potentially mimic more closely the biological context and thereby enhance enzyme function and stability.

In recent decades, a variety of patterning techniques have been developed and used for fabricating enzyme patterns.

Received: July 6, 2019

Accepted: October 14, 2019

Published: October 14, 2019

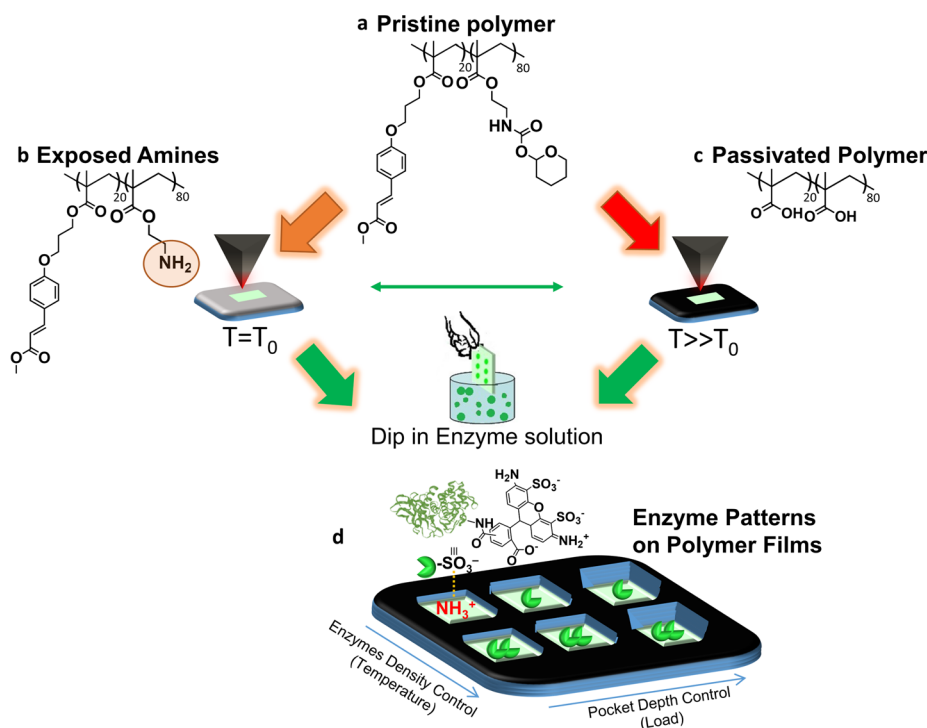


Figure 1. (a–c) Changes in chemical structure of the pristine polymer (a) upon heating with a tc-SPL hot tip at patterning temperatures of $T = T_0$ (~ 150 °C) to expose amine groups (b), and at $T \gg T_0$ to thermally hydrolyze the ester, forming carboxylic acid groups (c). (d) Schematic representation of the negatively charged sulfonated Alexa 488 conjugated thermolysin enzyme and its immobilization on positively charged amine patterns obtained in (b) with independent control of patterned topography and enzyme density by means of controlling temperature and load (pressure applied by tip on polymer). The black area surrounding the patterned pockets is the passivated region by high temperature patterning at $T \gg T_0$.

Among these techniques, microcontacting printing,^{2,9,12,13} optical lithography,^{14–16} and inkjet printing¹⁷ can provide enzyme patterns of micrometer size. Although enzyme patterns with sub-100 nm resolution have been generated using different methods, such as electron beam lithography (EBL),^{18–21} nanoimprint lithography (NIL),²² dip pen nanolithography (DPN),^{11,23,24} scanning probe lithography (SPL) methods,^{25–28} and various self-assembly processes,^{29–32} it is still an open challenge to achieve enzyme patterning using a simple and effective method which combines sub-10 nm resolution and high throughput. To date, only a few reports have demonstrated enzyme patterning with 10 nm resolution.^{23,29} For example, DPN has been able to generate an array of 10 nm Au nanoparticles with avidin–horseradish peroxidase attached.²³ However, the fabrication process involves multiple steps, i.e., patterning of block copolymer–metal ion complexes by DPN, reduction of the metal ions, removal of the polymer by plasma, annealing, and finally enzyme immobilization. Bottom-up self-assembly based patterning methods are well-known to generate sub-10 nm features.^{29,33,34} Sub-10 nm enzyme features were reported by immobilizing enzymes onto self-assembled 10 nm Pt islands deposited through dip-coating and electrochemical deposition.²⁹ However, this approach requires multiple steps and lacks specific control over the pattern configuration, biomolecule density, and topography, which limits its versatility for the fabrication of customized enzyme patterns. The ability to independently control surface chemistry and surface topography without affecting the other is of crucial importance in fabricating biosensors and bioreactors with well-controlled enzyme concentration and precisely defined geometry of the enzyme pockets and the surroundings.

Moreover, this dual control over chemistry and topography can significantly help the design of experiments to understand interfacial cell/extracellular matrix interactions, as well as the interaction of biomolecules with supporting surfaces.^{35–39} However, none of these techniques has the capability to independently control enzyme density and enzyme pocket geometry at the nanometer scale.

Here, we report on a method for nanopatterning enzyme pockets in a polymer film by controlling both enzyme density and pocket geometry with high throughput and sub-10 nm resolution. By using a commercial thermal-SPL system,⁴⁰ we demonstrate the direct patterning of amine groups, simultaneously with quasi-3D topography patterning of a thin polymer film. This process is followed by efficient single-step electrostatic enzyme immobilization by taking advantage of the attractive interaction between the negatively charged sulfonate moieties on functionalized enzymes and the positively charged amine patterns on the polymer surface in the aqueous environment. Using this approach, we obtain unprecedented sub-10 nm enzyme patterns with a top-down patterning method, together with independent control of surface chemistry and quasi-3D topography, and high throughput ($5.2 \times 10^4 \mu\text{m}^2/\text{h}$). Furthermore, we demonstrate a single step tc-SPL direct passivation strategy, which involves local thermal formation of carboxylic acid groups and does not require additional chemical functionalization to reduce nonspecific enzymes binding on the polymer surface. A model based on the reaction kinetics of amine deprotection and carboxylic acid formation is developed to describe the net density of immobilized sulfonated dyes and enzymes as a function of patterning temperature. The tc-SPL system employed here also

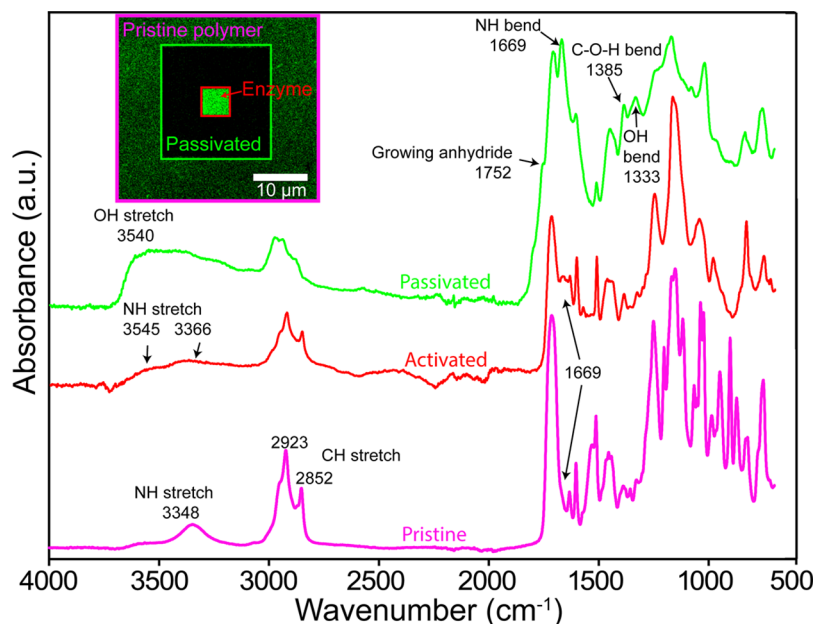


Figure 2. FTIR spectra of the pristine polymer film at room temperature (magenta), heated above the amine deprotection temperature ($T \sim 185$ °C, red spectra labeled as activated), and heated at the passivation temperature ($T \sim 240$ °C, green spectra labeled as passivated). The inset shows the confocal fluorescence image of selectively immobilized Alexa–thermolysin on an amine activated square pattern (marked with a red border, patterning temperature ~ 187 °C), within a passivated square pattern (marked with a green border, patterning temperature ~ 252 °C). The fluorescence intensity of the passivated region is around 8 times lower than the enzyme pattern. Here, the image contrast was tuned for clarity.

offers simultaneous *in situ* imaging of the topography before, during, and after patterning, enabling closed-loop lithography.⁴¹

2. RESULTS AND DISCUSSION

Micro- and nanoscale amine patterns are fabricated on the surface of a methacrylate-based copolymer film containing thermally labile tetrahydropyran (THP) carbamate protecting groups.^{42–44} The THP groups are selectively removed from the surface using a hot thermal-SPL nanotip, exposing primary amines. This concept, which was previously demonstrated by Riedo et al. using a custom-modified AFM equipped with thermal tips,^{42–44} is implemented here using a commercial thermal SPL system which allows for high throughput and mm² areas patterns (NanoFrazor^{40,45,46} from SwissLitho; see [Experimental Section](#)). The reaction scheme is depicted in [Figure 1a,b](#), where amine formation occurs through carbamate hydrolysis, when the surface of the methacrylate-based copolymer film is locally heated by tc-SPL at a temperature close to the amine deprotection temperature $T_0 \cong 150$ °C, as previously reported in the literature (see the [Experimental Section](#) for temperature calibration).^{42–44} However, as will be discussed later, here we also find that further heating at higher temperatures (>200 °C) and ambient humidity (RH $\sim 40\%$) results in significant hydrolysis of esters along the polymer chain, forming carboxylic acid groups ([Figure 1c](#)), which become negatively charged during enzyme incubation (pH ~ 7) and washing (pH ~ 7.4). These carboxylic acid groups can passivate the region patterned at higher temperature (i.e., repulse the enzymes). Unlike covalent immobilization through multistep biochemical-conjugation, as demonstrated previously in the literature for protein and DNA patterns,^{42–44} here we use a different strategy based on electrostatic interaction that allows for both chemical and topographical patterning, as well as passivation, directly, solely by tc-SPL. Specifically, enzyme

binding on the surface is driven by the electrostatic interaction in aqueous environment (pH ~ 7 and 7.4 for washing) between the negatively charged sulfonated Alexa-488 labeled enzymes and the positively charged exposed amines on the patterns.⁴⁷ In the passivated regions, the negatively charged carboxylate groups repel the negatively sulfonated Alexa-488 labeled enzymes by opposite interaction. Here, sulfonate functionalization of the enzymes is needed to immobilize them on the amine patterns, and we choose Alexa-based sulfonation so that it serves the dual purpose of immobilization and visualization. More details on the electrostatic immobilization are reported in the [Supporting Information \(SI\)](#). Bioconjugation and characterization of Alexa-488 labeled thermolysin is provided in the [SI](#). The term, Alexa-thermolysin, will be used to refer to the labeled enzymes in this report. After amine patterning by tc-SPL, Alexa–thermolysin can be immobilized onto the patterns by incubating the polymer films with Alexa–thermolysin solution (pH ~ 7) ([Figure 1d](#)). This one-step immobilization method avoids post-fabrication intermediate linker chemistry on the patterns and provides great simplicity, as well as effectiveness to immobilize the enzymes through noncovalent interactions.

2.1. Characterization of Film Passivation. A well-known challenge in biomolecular immobilization on patterned surfaces is their nonspecific binding, which compromises their binding selectivity. Most studies related to biomolecular patterning reduce the nonspecific binding by means of chemical functionalization of the unpatterned surface with antifouling residues, most commonly poly ethylene-glycol derivatives.^{10,22,23,48,49} Such passivation requires additional fabrication steps making the patterning process complex. In the following discussion, we demonstrate that tc-SPL patterning of the methacrylate-based copolymer at high temperatures in ambient humidity gives rise to a successful passivation because of the formation of carboxylic acid groups

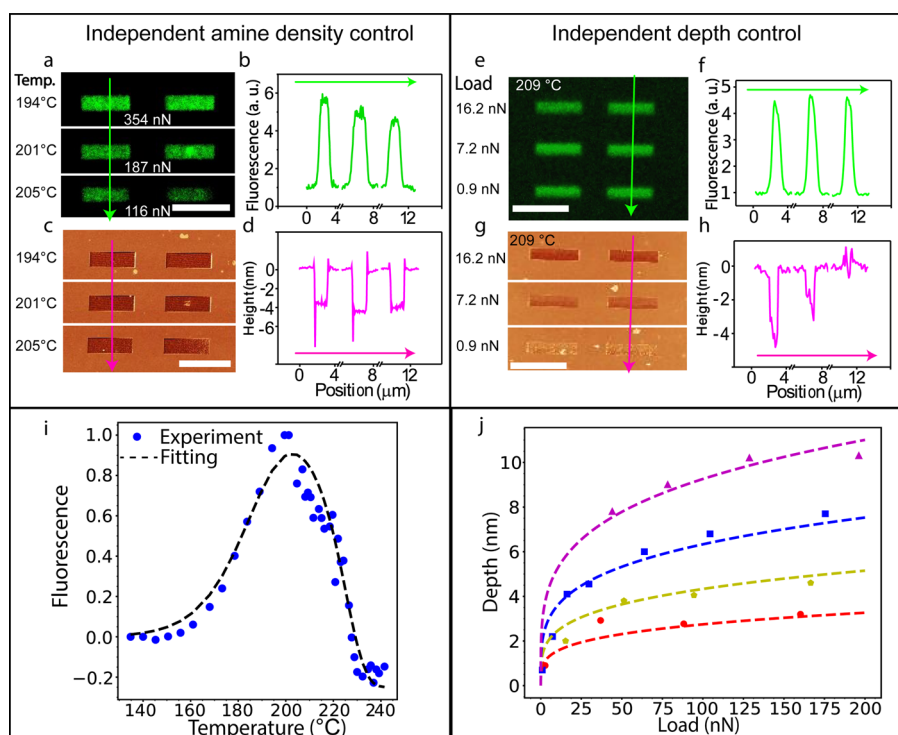


Figure 3. (a) Confocal fluorescence image and (b) corresponding emission intensity profile of rectangular patterns with different density of sulfonated Alexa 488 dye but similar topography, obtained by varying the patterning temperatures and load per unit area, i.e., tip pressure. (c) Corresponding AFM topography image and (d) cross-sectional height profile along the line drawn in (c) (z -scale = 19 nm) is shown. (e) Confocal fluorescence image and (f) corresponding emission intensity profile of rectangular patterns with similar density of sulfonated Alexa 488 dye (measured by fluorescence intensity) but different topography, obtained by varying the load during patterning at a constant temperature ($T = 209$ °C). (g) AFM topography image and (h) cross-sectional height profile along the line in (g) (z -scale = 17 nm). Scale bars for all images are 5 μm . (i) Fluorescence intensity of the patterns as a function of patterning temperature. The dashed line is the fitting using eq 5. (j) Pocket depth as a function of patterning load at different temperatures (from bottom to top, 179 °C, 195 °C, 209 °C, 223 °C). Data are fitted using a global model as eq 9.

(pK_a around 4), which become negatively charged during enzyme incubation ($\text{pH} \sim 7$) and washing ($\text{pH} \sim 7.4$). In the inset of Figure 2, we present the fluorescent image of a $4.5 \times 4.5 \mu\text{m}^2$ Alexa-thermolysin-immobilized pattern surrounded by a passivated $20 \times 20 \mu\text{m}^2$ squared area. The amine pattern is fabricated by tc-SPL with $T \sim 187$ °C, whereas the passivated area is produced by tc-SPL at $T \sim 252$ °C. While the unpatterned, pristine polymer shows a certain nonspecific binding (see the area marked in magenta), the passivated region (marked in green) clearly shows that the nonspecific binding is greatly reduced by this passivation method. In order to understand the mechanism behind this passivation at high temperature ($T \gg T_0$), pristine methacrylate-based copolymer films are heated at different temperatures and characterized by FTIR to assess changes in the chemical structure of the polymer surface. All measurements are performed at room temperature after heating. As shown in Figure 2 (magenta spectrum refers to room temperature sample; red for polymer film heated around 185 °C; green for polymer film heated around 240 °C), we observe that, as the temperature increases above the amine deprotection temperature, primary amines are formed. This is indicated by an elevated intensity around 1669 cm^{-1} (NH_2 bending; see magenta and red spectra in Figure 2) and by two shoulders at 3545 and 3366 cm^{-1} (NH_2 stretching, red spectra in Figure 2) as a broad band. The appearance of the broad band at around 3500 cm^{-1} in the red and green plots is due to OH stretching, possibly resulting from the formation of carboxylic groups, which form through the thermally assisted

ester hydrolysis along some side-chains in the polymer when heated in ambient humidity. This band falls in the same region of the amine stretching peaks and masks the NH_2 stretching peaks. Although a small amount of carboxyl groups form at temperatures close to T_0 , the pattern is mainly rich in amine groups which electrostatically bind the negatively charged Alexa-thermolysin enzymes in aqueous solution ($\text{pH} \sim 7$) (Figure 2, square enzyme pattern and red spectra). However, when the temperature is further increased to $T \gg T_0$ and $\text{RH} \sim 45\%$ (corresponding to a local temperature during patterning of more than 200 °C), more carboxylic acid groups seem to form along the polymer side-chains, as indicated by the enhancement in the OH band intensity around 3540 cm^{-1} (Figure 2b, green plot). Also, a clear shoulder appears next to the $\text{C}=\text{O}$ stretching peak at higher wavenumbers (1752 cm^{-1} , Figure 2, green plot). This can be ascribed to a certain amount of anhydride formed from the dehydration of carboxyl groups at these elevated temperatures, supporting the hypothesis that more carboxylic acid groups form. Two extra peaks also appear at 1385 and 1333 cm^{-1} after heating around 240 °C, which can be attributed to $\text{C}-\text{O}-\text{H}$ and OH in-plane bending of carboxylic acid groups. Since no nitrogen-related peak is overlapping in this region, these two peaks can be better evidence to distinguish between carboxylic acid groups and amines. We also remark that the formation of carboxylic acid groups during the thermal patterning process could be even more favorable than in the global heating procedure used here for the FTIR spectra, because water locally condenses at the

tip–surface meniscus^{50,51} and because of the large local pressure between tip and polymer.^{50,51} In aqueous solutions during enzyme immobilization (pH \sim 7) and washing (pH \sim 7.4), these carboxylic acid groups are readily deprotonated forming negatively charged carboxylates, which repel the negatively charged Alexa–thermolysin enzymes due to electrostatic repulsion, giving rise to an antifouling passivated polymer region (inset of Figure 2, darker square).

2.2. Independent Control of Topography and Enzyme Density in the Pockets. Since both surface chemistry and topography are relevant for interfacing biological components, it is desirable to control them independently.^{35,37–39} Such a control can be achieved by tc-SPL, as illustrated in Figure 3, and explained in the next paragraph. The control over sulfonated enzymes (Alexa–thermolysin) density inside pockets that have comparable size and depth is demonstrated in Figure 3a–d. The sulfonated enzyme density is indirectly probed by the fluorescence intensity of the immobilized Alexa 488 dye. Figure 3a shows confocal fluorescence images ($\lambda_{EM} = 515\text{--}600$ nm) of three sets of rectangular pockets which are tc-SPL patterned at three different tip temperatures as indicated in the figure. We observe that the fluorescence intensity decreases with increasing tip temperature indicating a decrease in the Alexa 488 density (Figure 3a,b). This decreased density with increasing temperature (from 194 to 205 °C) is in apparent disagreement with the concept that the amine density increases with temperature.^{42,43,52} Amine formation by carbamate deprotection is a thermally activated reaction; thus, the amine density in the pattern is expected to increase with the patterning temperature.⁴³ However, as discussed earlier, temperatures similar to or higher than the amine deprotection temperature can also trigger ester hydrolysis along the side-chains to form carboxylic acid groups (Figure 1c), which in turn can be deprotonated in the enzyme solution (pH \sim 7) and water solution (pH \sim 7.4) used for washing. Therefore, the increasing density of patterned negative charges results in a decreased density of immobilized negatively charged sulfonated Alexa 488 molecules in the pockets.

Increasing the tip temperature increases the indentation in the polymer and therefore the depth of the formed pocket. Thus, in order to maintain the same patterning depth with variable amine density, we decrease the overall patterning load, i.e., the pressure applied by the tc-SPL tip on the polymer surface during patterning, by reducing the capacitive force voltage (see the Experimental Section). As a result, the patterned rectangular pockets have the same depth (about 4 nm; see cross-sectional profile in Figure 3d). For the details on calibrating the patterning load, see SI. In summary, we can tune the temperature to vary the Alexa–thermolysin enzyme density in the patterned area, and simultaneously, we can also tune the load to maintain the same geometrical depth of the pocket. Accordingly, the corresponding AFM image (Figure 3c) of the same pockets, shown in Figure 3a before Alexa 488 incubation, shows that, for all the temperatures, the patterned rectangular pockets have the same depth of around 4 nm (Figure 3d).

To further investigate the temperature dependence of the density of the sulfonated molecules (Alexa 488 and Alexa–thermolysin enzymes) on the pattern, we collect the fluorescence intensity of multiple pockets patterned with increasing temperature (Figure 3i). Since the emitted fluorescence intensity per unit area, I , is proportional to the

density of the immobilized sulfonate-containing Alexa 488 on the pattern, this intensity I is used to quantify the density of the immobilized sulfonated molecules. We define $I_{rel} = \frac{N_{enzyme}}{N_{enzyme}^0}$ where N_{enzyme} is the density of the specifically and electrostatically immobilized sulfonated enzymes (as opposed to the nonspecific binding at the nonpatterned surface), and N_{enzyme}^0 is the maximum density of immobilized sulfonated enzymes, which will be discussed in more detail later. In Figure 3i, we plot $I_{rel} = \frac{I - I_{bg}}{I_{max} - I_{bg}}$, where I_{max} is the maximal measured fluorescence intensity per unit area, and I_{bg} is the background intensity per unit area. Figure 3i shows that the density of the sulfonated molecules which are immobilized on the patterned areas starts to increase at 151.8 °C, followed by a peak at around 196.8 °C; this behavior is due to amine deprotection (carbamate hydrolysis), and is in agreement with a previously reported work where dye molecules were bioconjugated to surface amine groups using a biotin–streptavidin functionalization.⁴² However, when the temperature is further increased, the density of the electrostatically immobilized sulfonated molecules on the patterns decreases, reaching a point where this density is even lower than that of the nonspecific adsorption on the background (seen as a negative intensity here). As discussed earlier, this decrease in the number of immobilized sulfonated molecules is due to the formation of more carboxyl groups as the temperature is further increased. To better elucidate the reaction mechanisms behind these processes, we model the reactions using the Arrhenius law. In the growing part of the curve (low temperatures, $T < 200$ °C), the density of the immobilized sulfonated molecules increases with temperature due to the amine deprotection. Therefore, the density depends on the contact temperature of the heated tip, the time of exposure, and the activation energy of amine deprotection. Since this is a unimolecular reaction, we model it using first-order chemical kinetics equations:

$$\frac{dN_{Amine}}{dt} = k(N_{Amine}^0 - N_{Amine}) \text{ with } k = A \exp\left(\frac{-E_a}{RT}\right) \quad (1)$$

where N_{Amine} is the amine density in the patterned areas, which, for low temperatures, can be considered to be proportional to the density of sulfonated molecules specifically and electrostatically immobilized at the amine groups, while N_{Amine}^0 is the maximum achievable amine density, t is the time, k is the rate constant, A is the Arrhenius constant, R is the gas constant, 8.3145 J/mol·K, T is the temperature at tip–polymer contact, and E_a is the activation energy of the reaction. Solving for N_{Amine} , we obtain

$$N_{Amine} = N_{Amine}^0 \left(1 - \exp\left(-At_d \exp\left(\frac{-E_a}{RT}\right)\right) \right) \quad (2)$$

where t_d is the tip–polymer dwelling time, calculated to be 1.4×10^{-4} s for a patterning speed of 0.2 mm/s, and N_{Amine}^0 corresponds to the maximum density of the deprotected amine groups.

To understand the decrease in the density of the immobilized sulfonated molecules with temperature, we consider two separate ester hydrolysis reactions (with different activation energies) that lead to the formation of carboxylic acid groups, which produce local repulsive negative charges during enzyme incubation and are responsible for the observed decrease in fluorescence intensity. As suggested by Figures 1

and 2, there are two possible ester hydrolysis producing carboxyl groups at high temperature on both the carbamate and cinnamate units of the copolymer. Thus, two different Arrhenius models are applied to both reactions. We assume that the amount of water participating in this reaction in the water meniscus at the tip–sample interface is abundant with respect to the ester so that the reaction follows first-order kinetics.⁵⁰ The first ester hydrolysis takes place on the cinnamate units close to the polymer backbone. The reaction model can be described as

$$N_{\text{COOH}}^1 = 0.25 \cdot N_{\text{Amine}}^0 \left(1 - \exp \left(-Bt_d \exp \left(\frac{-E_b}{RT} \right) \right) \right) \quad (3)$$

where N_{COOH}^1 is the density of carboxyl groups formed on the cinnamate units, E_b and B are the activation energy and the Arrhenius constant for this reaction, respectively, and $0.25 \cdot N_{\text{Amine}}^0$ is assumed to be the maximum carboxyl group density due to a 1:4 number ratio of cinnamate to carbamate in the polymer. Furthermore

$$N_{\text{COOH}}^2 = N_{\text{Amine}}^0 \left(1 - \exp \left(-Ct_d \exp \left(\frac{-E_c}{RT} \right) \right) \right) \quad (4)$$

where N_{COOH}^2 is the density of carboxyl groups formed on the carbamate units, C is the Arrhenius constant, and E_c is the corresponding activation energy. Here, since the carboxyl forms on the same units (carbamate) where amine forms first, it is assumed to have the same maximum product density (they have same number ratio, 1:1), i.e., N_{Amine}^0 . By combining the influence of all three reactions (see eqs 2–4) on the density of immobilized sulfonate enzymes (Alexa-thermolysin) in the patterned areas, we obtain a model that can fit the entire fluorescence–temperature curve, in both the growing and decaying regimes

$$I_{\text{rel}} = \frac{N_{\text{enzymes}}}{N_{\text{enzyme}}^0} = \frac{N_{\text{Amine}} - fN_{\text{COOH}}^1 - (1+f)N_{\text{COOH}}^2}{N_{\text{Amine}}^0} \quad (5)$$

where to model the attraction by positively charged amines and the repulsion by negatively charged carboxylates, we introduced a fitting parameter, f , employed to represent the ratio between the attraction and the repulsion exerted on the sulfonated molecules. It should be noted that when the carboxyl groups form on the carbamate units where the amines form at lower temperature, not only will the carboxyl groups repel a fraction of f sulfonated molecules, but the same amount of amines is also depleted; therefore, the third term in the model is multiplied by $-(1+f)$. We reiterate that since amine groups are positively charged upon protonated in water, they attract negatively charged sulfonated molecules, whereas negatively charged carboxylate groups repel the sulfonated molecules; therefore, in eq 5) they have opposite contribution to the net density of immobilized sulfonated molecules on the patterns. The model in eq 5 fits the measured fluorescence curve remarkably well, and yields the following results: $E_a \approx 135$ kJ/mol and $A \approx 1.6 \times 10^{19}$ s⁻¹, which are similar to the values obtained in previous work,⁴³ $E_b \approx 244$ kJ/mol, $B \approx 2.5 \times 10^{29}$ s⁻¹, $E_c \approx 262$ kJ/mol, $C \approx 2 \times 10^{31}$ s⁻¹, and $f \approx 0.2$. This reaction kinetics model indicates that as the temperature increases, the amine deprotection occurs first, followed by ester hydrolysis on the cinnamate units at higher T , forming a certain amount of carboxyl groups, which account for the

coexistence of the signature peaks of amine and carboxyl groups in the FTIR spectrum. As the temperature is further increased, more ester hydrolysis also occurs on the carbamate units, kicking away completely the amines and further reducing the density of the immobilized sulfonated molecules. When the temperature is even higher (~ 230 °C), the carboxyl formed on the pattern will dominate, repel the enzymes, and passivate the surface compared to the unpatterned background region.

To investigate the ability to maintain a constant density of immobilized enzymes while varying the pocket pattern geometry, i.e., shape, size, and depth, we use a constant tip temperature (~ 209 °C) but different normal loads applied by the tip to the polymer surface (0.9–16.2 nN) (Figure 3e–h). Indeed, the fluorescence intensity (Figure 3f) and cross-sectional height profiles of these rectangular pockets (Figure 3h) show similar fluorescence intensity but different depths; more precisely, the depth increases with increasing load. In order to precisely control the pocket depth, we investigate the relationship between patterning load, temperature, and the resulting pocket depth. By varying the patterning load and temperature, pockets with a variety of depths are fabricated. The resulting depth values as a function of patterning load at different constant temperature are plotted in Figure 3j. From Figure 3j, it is clearly shown that for a fixed temperature the pocket depth first increases rapidly with load, and then increases slowly. On the other hand, for a fixed load the pocket depth increases significantly with temperature, which is mainly due to the softening of the polymer with the increasing temperature. To model such dependence of the pocket depth on the patterning load and temperature, we refer to the classical contact mechanics Hertz model.^{53,54} According to the classical Hertz elastic contact model, the indentation depth of a sphere in a semi-infinite flat substrate is a function of the load, following the equation

$$z_{\text{indent}} = \left(\frac{3L}{4\sqrt{RE^*}} \right)^{2/3} \quad (6)$$

where z_{indent} is the indentation depth, L is the tip load, R is the radius of the tip, and E^* is the effective Young's modulus of the tip–polymer system.^{53,54} However, the Hertz contact elastic model is valid only for a purely elastic indentation of a sphere into a semi-infinite flat substrate. In our experiments, although the tip is a rigid silicon sphere, the substrate is a soft viscoelastic polymer. Therefore, the indentation is no longer a pure elastic process but a heat-assisted elasto-plastic process,^{55,56} which leads to a deviation from the Hertz theory. A more general model to describe the tip–polymer system presented here, involving elasto-plastic indentations, is given by the following relationship

$$d \propto \left(\frac{L}{E(T)} \right)^n \quad (7)$$

where d is the pocket depth and $E(T)$ is the temperature-dependent Young's modulus of the polymer, which is much smaller than that of the silicon tip. The exponent n depends on the mechanical behavior of the individual material undergoing the plastic deformation.^{55,56} We also notice that this model may be valid only when the depth is much smaller than the polymer film thickness. If the film is too thin or the pattern depth approaches the film thickness, the heated tip is in a position very close to the Si substrate leading to significant heat dissipation. Assuming that we are in a regime where the

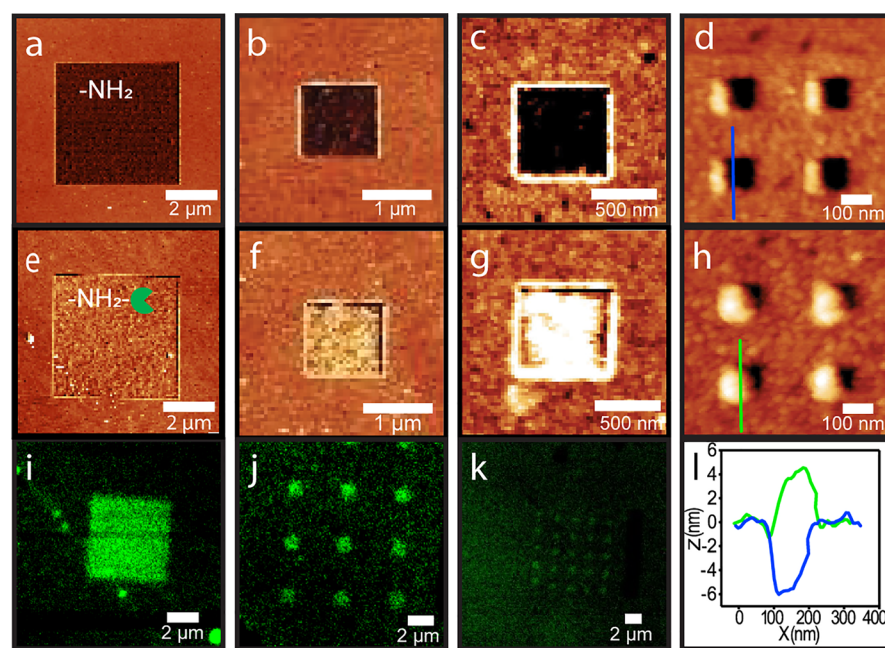


Figure 4. Series of AFM images collected (a–d) before and (e–h) after thermolysin immobilization on a polymer film (z-scale is 16 nm (a), 11 nm (b), 4 nm (c), 12 nm (d), 9 nm (e), 9 nm (f), 5 nm (g), 12 nm (h)). (i,j,k) Confocal fluorescence images corresponding to patterns in (e,f,g), respectively. (l) Cross-sectional profiles from (d) (blue line) and h (green line).

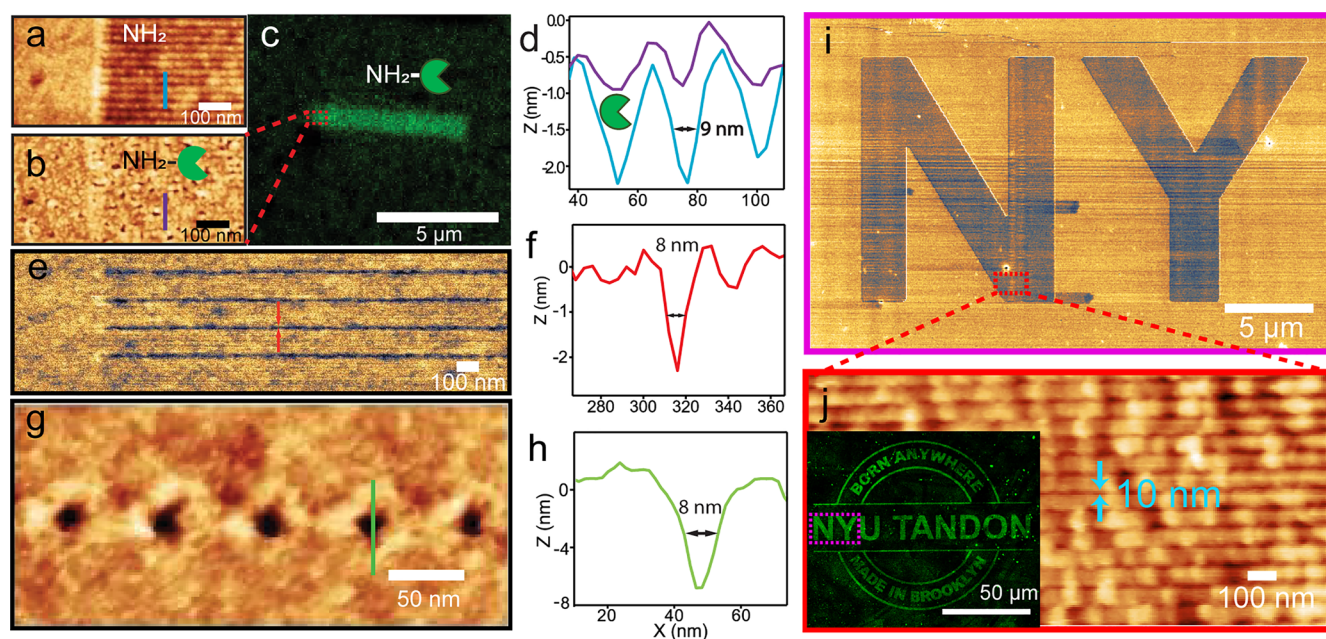


Figure 5. (a,b) AFM topography of part of a rectangular area of size $1 \times 5 \mu\text{m}^2$ made up of closely packed 9-nm-wide lines of amine pattern before (a) and after (b) Alexa–thermolysin immobilization (z-scale is 10 nm). (c) Corresponding fluorescence image of the rectangular area, containing electrostatically bound Alexa–thermolysin. (d) Cross-sectional profile corresponding to the light blue line in (a) and the violet line in (b), showing fwhm = 9 nm. (e) Thermal *in situ* topography imaging of as-patterned amine single lines. (g) AFM topography of as-patterned amine dots. (f,h) Corresponding cross-sectional profiles of the patterns in (e) and (g) showing sub-10 nm patterning resolution. (i) Thermal *in situ* topography imaging of patterned “NY” from logo pattern of NYU Tandon as shown in inset of (j). (j) AFM topography image of the zoomed-in area in (i), showing high resolution single-line patterning of 10 nm fwhm. Inset is the fluorescence image of the Alexa–thermolysin enzyme pattern of NYU Tandon logo. Permission to use logo was granted by the New York University Trademark Licensing.

temperature is below the glass transition temperature of the polymer, the temperature-dependent polymer Young’s modulus in this regime can be approximated as follows:⁵⁷

$$\log E(T) = \log E(T_{\text{RT}}) - s \cdot (T - T_{\text{RT}}) \quad (8)$$

where T_{RT} is the room temperature, $E(T_{\text{RT}})$ is the Young’s modulus at room temperature, and s is a parameter related to the temperature sensitivity of the material. The detailed study of the temperature dependence of the Young’s modulus of this polymer is beyond the scope of this work. By substituting eq 8 into eq 7, we obtain

$$d \propto \left(\frac{L}{E(T_{RT}) \cdot e^{-s \cdot (T-20)}} \right)^n \quad \text{and therefore}$$

$$d \propto \left(\frac{L}{e^{-s \cdot (T-20)}} \right)^n \quad (9)$$

By using this relationship, we fit the data in Figure 3j (dotted line) obtaining a good agreement with the fitting parameters $n = \frac{1}{4}$ and $s = 0.11 \text{ } ^\circ\text{C}^{-1}$. This model and related data points demonstrate the ability of tc-SPL to control with 1 nm precision the depth of the enzyme pockets.

2.3. Enzyme Immobilization on the Micro- and Nanopatterned Pockets. Figure 4a–h shows Alexa–thermolysin enzymes immobilized on a series of square-shaped pockets of exposed amines with areas ranging from $5 \times 5 \text{ } \mu\text{m}^2$ to $0.1 \times 0.1 \text{ } \mu\text{m}^2$. This is demonstrated with fluorescence microscopy images and AFM topography images obtained before (Figure 4a–d) and after (Figure 4e–h) incubation of the amine-patterned polymer surface with Alexa–thermolysin enzyme solutions. The corresponding confocal fluorescence images of the pockets filled with enzymes are shown in Figure 4i–k. The fluorescent image of the $0.1 \times 0.1 \text{ } \mu\text{m}^2$ enzyme pockets could not be obtained with good visibility due to the limited resolution of the confocal fluorescence microscope. To confirm the presence of enzymes in these smaller pockets, we use AFM to image the pockets before (Figure 4d) and after (Figure 4h) enzyme immobilization. In Figure 4l we show the corresponding cross-sectional height profiles (blue line in Figure 4d, green line in Figure 4h). Comparison of the pockets' topography before and after Alexa–thermolysin incubation clearly demonstrates that the pockets produced by tc-SPL are filled by enzymes. The topographic height difference of about 8 nm is comparable with the expected diameter of a single Alexa–thermolysin enzyme molecule (around 6 nm, see Figure S2). Comparison done at multiple positions on different samples as shown in Figure 4 results in height differences of about 5–8 nm after enzyme incubation, confirming that a monolayer of enzyme is immobilized on the surface of the patterns.

An alternative strategy to image small features by confocal fluorescence microscopy is to pattern by tc-SPL a $1 \times 5 \text{ } \mu\text{m}^2$ area with closely packed enzymes lines having a full width at half-maximum (fwhm) of 9 nm and a length of $1 \text{ } \mu\text{m}$ (Figure 5a), followed by incubation with the Alexa–thermolysin solution. The fluorescence imaging of such a pattern shows enhanced fluorescence emission from this patterned area, indicating that Alexa–thermolysin enzymes are indeed immobilized in the pocket lines in the patterned area (Figure 5c), as also confirmed by the AFM topographic images before (Figure 5a) and after incubation (Figure 5b and cross-sectional profiles in Figure 5d). To further demonstrate the versatility of tc-SPL for high spatial resolution patterning in the sub-10 nm range, we pattern isolated sub-10 nm lines (Figure 5e) and dots (Figure 5g). Both lines and the dots exhibit a fwhm of 8 nm in the corresponding cross-sectional profiles (Figure 5f and h, respectively), very close to the size of a single enzyme (~ 6 nm), confirming the capacity to achieve sub-10 nm and single enzyme patterning resolution by tc-SPL. Furthermore, our method is capable of combining large-scale ($0.13 \times 0.1 \text{ mm}^2$) and high-throughput ($5.2 \times 10^4 \text{ } \mu\text{m}^2/\text{h}$) patterning of enzymes with 10 nm detailed features (see Figure 5i,j). This indicates

the remarkable potential of this method for high-throughput nanofabrication of miniature biochips.

3. CONCLUSION

In conclusion, we demonstrate sub-10 nm enzyme nanopatterning on a polymer surface by using a commercial tc-SPL system. Our patterning scheme allows enzyme immobilization into amine pockets patterned by tc-SPL in a single step (incubation in the enzyme solution) without any post-patterning treatment. This is realized through the electrostatic attraction between the negatively charged sulfonate-functionalized enzymes and the positively charged amine groups in aqueous conditions. By tuning the patterning temperature and load applied by the tip to the polymer surface, we achieve independent control of pockets' quasi-3D geometry and enzyme density, which are both of significant importance for cell behavior and biomolecule recognition studies. We obtain 1 nm resolution in depth, and 8 nm resolution in lateral direction, respectively, over areas of mm^2 . In addition, the nonspecific binding on the pristine polymer surface can be effectively reduced by taking advantage of the formation of carboxyl groups through ester hydrolysis at high patterning temperatures. These groups are negatively charged in aqueous solution and thus repel the negatively charged Alexa–thermolysin enzymes. This strategy is a facile and effective way to passivate areas of these polymer films against biomolecule adsorption without the need of any other surface treatment. Finally, the method presented here of immobilizing biomolecules and passivating surfaces through electrostatic interaction can be generalized for the immobilization of a variety of similarly sulfonate-functionalized biomolecules, demonstrating great versatility and effectiveness. This tc-SPL-based enzyme nanopatterning approach also has the potential to be scaled up for industrial nanomanufacturing using multiple tip arrays and taking advantage of its throughput (up to $10^5 \text{ } \mu\text{m}^2/\text{s}$ for a single tip). Compared to other nanofabrication techniques that can achieve sub-10 nm enzyme/protein patterns, this method is additionally advantageous in the following aspects: (1) simultaneous patterning and *in situ* imaging (Figure 5e,i and Figure S7) with closed-loop lithography; (2) direct immobilization of enzymes on the amine patterns without the need of multiple intermediate steps; (3) wide possibility of generating quasi-3D arbitrary patterns with 1 nm resolution in *z*-direction (Figure S7b); (4) without the need of a prefabricated mold surface for each design, as required by NIL; (5) scalability and potential parallelization using multiple tips;⁵⁸ (6) electrostatic interaction for immobilization as a modular chemical strategy which can be easily adapted for a range of biomolecules. All the above features demonstrate the great simplicity and effectiveness of this approach, and will have significant impact on a variety of fields such as bionanotechnology, reaction nanochemistry, biochemistry, and cell biology.

4. EXPERIMENTAL SECTION

Polymer and Surface Preparation. The polymer used for film preparation is a poly(methacrylate) copolymer: poly((tetrahydropyran-2-yl *N*-(2-methacryloyloxyethyl) carbamate)-*b*-(methyl 4-(3-methacryloyloxypropoxy) cinnamate)). Full details on the synthesis can be found in the literature.⁵⁹ The polymer contains thermally labile tetrahydropyran carbamate groups along its side-chain, which upon heating at the deprotection temperature ($T_0 \sim 150\text{--}200 \text{ } ^\circ\text{C}$), dissociate and expose the primary amines.^{42–44}

Polymer solutions at the concentration of 2.5 mg/mL were prepared in chloroform. For obtaining the polymer films, the polymer solution was spin-coated onto the Si substrate (1500 rpm, 60s) followed by a quick baking (50 °C, 1 min). Under these conditions, the resulting film thickness ranges from 20 to 30 nm.

Thermochemical SPL. Patterning of the polymer films was performed using a commercial tc-SPL system (NanoFrazor, fLitho AG, Switzerland) which utilizes a silicon thermal cantilever for inducing a local amine deprotection reaction. The thermal cantilever comprises a nanosize tip heated by a resistive heater for thermal patterning, and a separate thermal reading sensor for topography imaging. During thermal patterning, the tip is heated to a certain temperature calibrated automatically by the NanoFrazor software by fitting the knee point from the current–voltage curve to the theoretical value for doped silicon.⁶⁰ At given temperature and cantilever height above the sample, the patterning load is controlled by the capacitive force between the cantilever and substrate that drives the cantilever to bend toward the sample. Notably, once the tip heater is switched on, an extra cantilever bending occurs due to the nonuniform temperature distribution, causing extra load to the sample. To determine the load during the patterning process, we calibrate the cantilever deflection resulting from both capacitive force and temperature. By using the known cantilever spring constant and the distance between the cantilever and the sample surface, the load can be calibrated. The details on measuring the cantilever deflection and load calibration are reported in the SI. During the patterning, the thermal reading sensor probes the topography of the patterned structure right after each patterning line when retracing back in contact mode, which leads to the simultaneous patterning and imaging capability of the NanoFrazor system as well as a closed feedback loop correction.⁶¹

In this work, the resistively heated tip locally heats the polymer films over the amine deprotection temperature ($T_0 \sim 150$ °C). Patterning is performed in contact mode with a tip dwell time of 140 μ s (speed: 0.2 mm/s) and pixel size of 30 nm. For high-throughput patterning in Figure 5j, tip dwell time is 50 μ s (speed: 1 mm/s) and pixel size is 50 nm. The surface density of exposed amines is controlled by varying the tip temperature while keeping a constant tip dwell time and pixel size. The passivated areas with reduced nonspecific binding are patterned with $T_{\text{contact}} \sim 230$ –260 °C. The contact temperature at the tip–sample interface cannot be directly measured due to a reduced heat transport from the heater to the conical tip. To estimate the tip–sample contact temperature, a heating efficiency between the heater and the sample surface was derived with the value of 0.24. The tip–sample contact temperature was then estimated based on the following equation $T_{\text{contact}} = 0.24(T_{\text{heater}} - T_{\text{RT}}) + T_{\text{RT}}$, where T_{RT} is the room temperature and T_{heater} is the heater temperature.^{41,62,63} In this work, the NanoFrazor was operated in the pulsed heating mode by which the tip was heated intermittently in order to extend its lifetime. The typical settings for heat pulses and capacitive force pulses were 120 and 100 μ s, respectively.

Synthesis of Alexa–Thermolysin Enzymes. Thermolysin (4 mg, from *Bacillus Thermoproteolyticus* Rokko) was dissolved in 3 mL water (pH is adjusted to 8) and Alexa-488 NHS solution in DMSO (60 μ L, 2 mM) was added. The solution was then left in a shaker for 2 h. After dialysis of the solution (one-day dialysis with regularly changing of water every 3–4 h) to wash off any unreacted dye (dialysis membrane with Molecular Weight cut off = 3500 Da), the remaining solution was lyophilized to obtain Alexa-488 conjugated Thermolysin (Alexa–thermolysin). The product formation was confirmed by mass spectrometry (MALDI).

Dyes and Enzymes Immobilization. Alexa 488 dyes were immobilized onto the tc-SPL patterns by incubating the polymer film with Alexa 488 solution (100 nM, 100 μ L) in water for 45 min. After incubation, the surface was rinsed with deionized (DI) water and then dried with N_2 . Alexa–thermolysin enzyme immobilization was achieved by incubating the polymer film in Alexa 488–thermolysin conjugate solution in water (30 μ L, 1 mg/mL) for 1 h. After incubation, the surface was rinsed with DI water and dried with N_2 .

Fluorescence Resonance Energy Transfer (FRET)-Peptide Based Assay. The FRET substrate Glu (EDANS)-Gly-Thr-Leu-Gly-Lys (DABCYL) was purchased from China Peptides and dissolved in dimethyl sulfoxide (DMSO) to obtain a 10 mM stock solution. Appropriate amount of this stock solution was injected into phosphate buffer (100 mM, pH = 7.4) to obtain a final working concentration of 0.5 μ M. Thermolysin, immobilized on the patterned polymer surface, was inserted in a 10 mm quartz cuvette containing the FRET solution, and fluorescence intensity was monitored at 520 nm upon excitation at 340 nm.

Fluorescence Microscopy Imaging. Fluorescence imaging was performed using laser scanning confocal microscopy (Zeiss LSM 880 Airyscan (Figures 3 to 5) and Leica TCS SP8 STED 3X (Figure 2)), with excitation laser wavelength $\lambda_{\text{EX}} = 488$ nm and emission detection range $\lambda_{\text{EM}} = 510$ –600 nm. The optical contrast in different fluorescent images was tuned for better visibility by standard image processing using ImageJ. The fluorescence intensity in Figure 3b and f is calculated as $I_{\text{pattern}}/I_{\text{background}}$, where I_{pattern} and $I_{\text{background}}$ are absolute intensity values of patterns and background, respectively.

AFM Characterization. All AFM experiments were performed on a Bruker MultiMode 8 AFM using tapping mode. Flattening and z-scale adjustment of AFM images were performed with Gwyddion software.

■ ASSOCIATED CONTENT

📄 Supporting Information

The Supporting Information is available free of charge on the ACS Publications website at DOI: 10.1021/acsami.9b11844.

Confirmation of electrostatic immobilization; Enzyme size characterization; Characterization of Alexa–Thermolysin conjugates; Enzyme activity characterization; Simultaneous patterning and *in situ* imaging of NanoFrazor; Patterning load calibration (PDF)

■ AUTHOR INFORMATION

Corresponding Authors

*E-mail: elisa.riedo@nyu.edu.

*E-mail: Rein.Ulijn@asrc.cuny.edu.

ORCID

Xiangyu Liu: 0000-0001-7010-6554

Edoardo Albisetti: 0000-0002-8134-0482

Elizabeth Elacqua: 0000-0002-1239-9560

Marcus Weck: 0000-0002-6486-4268

Rein V. Ulijn: 0000-0002-7138-1213

Elisa Riedo: 0000-0002-2423-8801

Author Contributions

The manuscript was written through contributions of all authors. All authors have given approval to the final version of the manuscript.

Notes

The authors declare no competing financial interest.

■ ACKNOWLEDGMENTS

The authors acknowledge support from the US Army Research 719 Office (proposal number 69180-CH), the Office of Basic 720 Energy Sciences of the US Department of Energy, and the 721 National Science Foundation (CHE-1506890, K.B.M., E.E., 722 M.W.). This work was also supported partially by the MRSEC Program of the National Science Foundation under Award Number DMR-1420073.

REFERENCES

- (1) Riemenschneider, L.; Blank, S.; Radmacher, M. Enzyme-Assisted Nanolithography. *Nano Lett.* **2005**, *5*, 1643–1646.
- (2) Kargl, R.; Mohan, T.; Köstler, S.; Spirk, S.; Doliška, A.; Stana-Kleinschek, K.; Ribitsch, V. Functional Patterning of Biopolymer Thin Films Using Enzymes and Lithographic Methods. *Adv. Funct. Mater.* **2013**, *23*, 308–315.
- (3) Miles, E. W.; Rhee, S.; Davies, D. R. The Molecular Basis of Substrate Channeling. *J. Biol. Chem.* **1999**, *274*, 12193–12196.
- (4) Sassolas, A.; Blum, L. J.; Leca-Bouvier, B. D. Immobilization Strategies to Develop Enzymatic Biosensors. *Biotechnol. Adv.* **2012**, *30*, 489–511.
- (5) Rissin, D. M.; Kan, C. W.; Campbell, T. G.; Howes, S. C.; Fournier, D. R.; Song, L.; Piech, T.; Patel, P. P.; Chang, L.; Rivnak, A. J. Single-Molecule Enzyme-Linked Immunosorbent Assay Detects Serum Proteins at Subfemtomolar Concentrations. *Nat. Biotechnol.* **2010**, *28*, 595–599.
- (6) Li, Z.; Liu, X.; Zhang, Z. Preparation of F₀F₁-ATPase Nanoarray by Dip-Pen Nanolithography and Its Application as Biosensors. *IEEE Trans Nanobioscience* **2009**, *7*, 194–199.
- (7) Küchler, A.; Yoshimoto, M.; Luginbühl, S.; Mavelli, F.; Walde, P. Enzymatic Reactions in Confined Environments. *Nat. Nanotechnol.* **2016**, *11*, 409–420.
- (8) De La Rica, R.; Matsui, H. Urease as a Nanoreactor for Growing Crystalline ZnO Nanoshells at Room Temperature. *Angew. Chem., Int. Ed.* **2008**, *47*, 5415–5417.
- (9) Fabijanic, K. I.; Perez-Castillejos, R.; Matsui, H. Direct Enzyme Patterning with Microcontact Printing and the Growth of ZnO Nanoparticles on the Catalytic Templates at Room Temperature. *J. Mater. Chem.* **2011**, *21*, 16877–16879.
- (10) Lee, K.-B.; Lim, J.-H.; Mirkin, C. A. Protein Nanostructures Formed Via Direct-Write Dip-Pen Nanolithography. *J. Am. Chem. Soc.* **2003**, *125*, 5588–5589.
- (11) Li, H.; He, Q.; Wang, X.; Lu, G.; Liusman, C.; Li, B.; Boey, F.; Venkatraman, S. S.; Zhang, H. Nanoscale-Controlled Enzymatic Degradation of Poly (L-Lactic Acid) Films Using Dip-Pen Nanolithography. *Small* **2011**, *7*, 226–229.
- (12) Buhl, M.; Vonhören, B.; Ravoo, B. J. Immobilization of Enzymes Via Microcontact Printing and Thiol–Ene Click Chemistry. *Bioconjugate Chem.* **2015**, *26*, 1017–1020.
- (13) Guyomard-Lack, A.; Delorme, N.; Moreau, C.; Bardeau, J.-F.; Cathala, B. Site-Selective Surface Modification Using Enzymatic Soft Lithography. *Langmuir* **2011**, *27*, 7629–7634.
- (14) Lee, Y.-N.; Horio, T.; Okumura, K.; Iwata, T.; Takahashi, K.; Ishida, M.; Sawada, K. In *Patterning an Enzyme-Membrane of Bio-Image Sensor Using Lithography Technique*; SENSORS 2015 IEEE, Busan, South Korea, Nov 1–4, 2015.
- (15) Marchesan, S.; Easton, C. D.; Styan, K. E.; Leech, P.; Gengenbach, T. R.; Forsythe, J. S.; Hartley, P. G. Su-8 Photolithography on Reactive Plasma Thin-Films: Coated Microwells for Peptide Display. *Colloids Surf., B* **2013**, *108*, 313–321.
- (16) Alvarado, R. E.; Nguyen, H. T.; Pepin-Donat, B.; Lombard, C.; Roupioz, Y.; Leroy, L. Optically Assisted Surface Functionalization for Protein Arraying in Aqueous Media. *Langmuir* **2017**, *33*, 10511–10516.
- (17) Gdor, E.; Shemesh, S.; Magdassi, S.; Mandler, D. Multienzyme Inkjet Printed 2d Arrays. *ACS Appl. Mater. Interfaces* **2015**, *7*, 17985–17992.
- (18) Kim, S.; Marelli, B.; Brenckle, M. A.; Mitropoulos, A. N.; Gil, E. S.; Tsioris, K.; Tao, H.; Kaplan, D. L.; Omenetto, F. G. All-Water-Based Electron-Beam Lithography Using Silk as a Resist. *Nat. Nanotechnol.* **2014**, *9*, 306–310.
- (19) Bat, E.; Lee, J.; Lau, U. Y.; Maynard, H. D. Trehalose Glycopolymer Resists Allow Direct Writing of Protein Patterns by Electron-Beam Lithography. *Nat. Commun.* **2015**, *6*, 6654.
- (20) Lockhart, J. N.; Hmelo, A. B.; Harth, E. Electron Beam Lithography of Poly(Glycidol) Nanogels for Immobilization of a Three-Enzyme Cascade. *Polym. Chem.* **2018**, *9*, 637–645.
- (21) Mancini, R. J.; Paluck, S. J.; Bat, E.; Maynard, H. D. Encapsulated Hydrogels by E-Beam Lithography and Their Use in Enzyme Cascade Reactions. *Langmuir* **2016**, *32*, 4043–4051.
- (22) Merino, S.; Retolaza, A.; Trabadelo, V.; Cruz, A.; Heredia, P.; Alduncin, J. A.; Mecerreyes, D.; Fernández-Cuesta, I.; Borrisé, X.; Pérez-Murano, F. Protein Patterning on the Micro- and Nanoscale by Thermal Nanoimprint Lithography on a New Functionalized Copolymer. *J. Vac. Sci. Technol., B: Microelectron. Nanometer Struct.–Process., Meas., Phenom* **2009**, *27*, 2439–2443.
- (23) Chai, J.; Wong, L. S.; Giam, L.; Mirkin, C. A. Single-Molecule Protein Arrays Enabled by Scanning Probe Block Copolymer Lithography. *Proc. Natl. Acad. Sci. U. S. A.* **2011**, *108*, 19521–19525.
- (24) Xie, Z.; Chen, C.; Zhou, X.; Gao, T.; Liu, D.; Miao, Q.; Zheng, Z. Massively Parallel Patterning of Complex 2d and 3d Functional Polymer Brushes by Polymer Pen Lithography. *ACS Appl. Mater. Interfaces* **2014**, *6*, 11955–11964.
- (25) De La Rica, R.; Matsui, H. Biomimetic Conformation-Specific Assembly of Proteins at Artificial Binding Sites Nanopatterned on Silicon. *J. Am. Chem. Soc.* **2009**, *131*, 14180–14181.
- (26) Shi, J.; Chen, J.; Cremer, P. S. Sub-100 Nm Patterning of Supported Bilayers by Nanoshaving Lithography. *J. Am. Chem. Soc.* **2008**, *130*, 2718–2719.
- (27) Martinez, R. V.; Martinez, J.; Chiesa, M.; Garcia, R.; Coronado, E.; Pinilla-Cienfuegos, E.; Tatay, S. Large-Scale Nanopatterning of Single Proteins Used as Carriers of Magnetic Nanoparticles. *Adv. Mater.* **2010**, *22*, 588–591.
- (28) Garcia, R.; Knoll, A. W.; Riedo, E. Advanced Scanning Probe Lithography. *Nat. Nanotechnol.* **2014**, *9*, 577–587.
- (29) Gajdzik, J.; Lenz, J.; Natter, H.; Hempelmann, R.; Kohring, G. W.; Giffhorn, F.; Manolova, M.; Kolb, D. M. Enzyme Immobilisation on Self-Organised Nanopatterned Electrode Surfaces. *Phys. Chem. Chem. Phys.* **2010**, *12*, 12604–12607.
- (30) Samanta, D.; Sarkar, A. Immobilization of Bio-Macromolecules on Self-Assembled Monolayers: Methods and Sensor Applications. *Chem. Soc. Rev.* **2011**, *40*, 2567–2592.
- (31) Fu, J.; Liu, M.; Liu, Y.; Woodbury, N. W.; Yan, H. Interenzyme Substrate Diffusion for an Enzyme Cascade Organized on Spatially Addressable DNA Nanostructures. *J. Am. Chem. Soc.* **2012**, *134*, 5516–5519.
- (32) Wollenberg, L. A.; Jett, J. E.; Wu, Y.; Flora, D. R.; Wu, N.; Tracy, T. S.; Gannett, P. M. Selective Filling of Nanowells in Nanowell Arrays Fabricated Using Polystyrene Nanosphere Lithography with Cytochrome P450 Enzymes. *Nanotechnology* **2012**, *23*, 385101.
- (33) Suh, H. S.; Moni, P.; Xiong, S.; Ocola, L. E.; Zaluzec, N. J.; Gleason, K. K.; Nealey, P. F. Sub-10-Nm Patterning Via Directed Self-Assembly of Block Copolymer Films with a Vapour-Phase Deposited Topcoat. *Nat. Nanotechnol.* **2017**, *12*, 575–581.
- (34) Rinker, S.; Ke, Y.; Liu, Y.; Chhabra, R.; Yan, H. Self-Assembled DNA Nanostructures for Distance-Dependent Multivalent Ligand–Protein Binding. *Nat. Nanotechnol.* **2008**, *3*, 418–422.
- (35) Dalby, M. J.; Gadegaard, N.; Oreffo, R. O. Harnessing Nanotopography and Integrin–Matrix Interactions to Influence Stem Cell Fate. *Nat. Mater.* **2014**, *13*, 558–569.
- (36) Li, D.; Zheng, Q.; Wang, Y.; Chen, H. Combining Surface Topography with Polymer Chemistry: Exploring New Interfacial Biological Phenomena. *Polym. Chem.* **2014**, *5*, 14–24.
- (37) Kim, D.-H.; Provenzano, P. P.; Smith, C. L.; Levchenko, A. Matrix Nanotopography as a Regulator of Cell Function. *J. Cell Biol.* **2012**, *197*, 351–360.
- (38) Parent, C. A.; Devreotes, P. N. A Cell's Sense of Direction. *Science* **1999**, *284*, 765–770.
- (39) Yang, J.; Rose, F. R.; Gadegaard, N.; Alexander, M. R. A High-Throughput Assay of Cell-Surface Interactions Using Topographical and Chemical Gradients. *Adv. Mater.* **2009**, *21*, 300–304.
- (40) Zheng, X.; Calò, A.; Albisetti, E.; Liu, X.; Alharbi, A. S. M.; Arefe, G.; Liu, X.; Spieser, M.; Yoo, W. J.; Taniguchi, T.; Watanabe, K.; Aruta, C.; Ciarrocchi, A.; Kis, A.; Lee, B. S.; Lipson, M.; Hone, J.; Shahjerdi, D.; Riedo, E. Patterning Metal Contacts on Monolayer

Mos 2 with Vanishing Schottky Barriers Using Thermal Nanolithography. *Nat. Electron.* **2019**, *2*, 17–25.

(41) Zimmermann, S. T.; Balkenende, D. W.; Lavrenova, A.; Weder, C.; Brugger, J. r. Nanopatterning of a Stimuli-Responsive Fluorescent Supramolecular Polymer by Thermal Scanning Probe Lithography. *ACS Appl. Mater. Interfaces* **2017**, *9*, 41454–41461.

(42) Albiseti, E.; Carroll, K.; Lu, X.; Curtis, J.; Petti, D.; Bertacco, R.; Riedo, E. Thermochemical Scanning Probe Lithography of Protein Gradients at the Nanoscale. *Nanotechnology* **2016**, *27*, 315302.

(43) Carroll, K. M.; Giordano, A. J.; Wang, D.; Kodali, V. K.; Scrimgeour, J.; King, W. P.; Marder, S. R.; Riedo, E.; Curtis, J. E. Fabricating Nanoscale Chemical Gradients with Thermochemical Nanolithography. *Langmuir* **2013**, *29*, 8675–8682.

(44) Wang, D.; Kodali, V. K.; Underwood, W. D., II; Jarvholm, J. E.; Okada, T.; Jones, S. C.; Rumi, M.; Dai, Z.; King, W. P.; Marder, S. R. Thermochemical Nanolithography of Multifunctional Nanotemplates for Assembling Nano-Objects. *Adv. Funct. Mater.* **2009**, *19*, 3696–3702.

(45) Pires, D.; Hedrick, J. L.; Silva, A. D.; Frommer, J.; Gotsmann, B.; Wolf, H.; Despont, M.; Duerig, U.; Knoll, A. W. Nanoscale Three-Dimensional Patterning of Molecular Resists by Scanning Probes. *Science* **2010**, *328*, 732–735.

(46) Szoszkiewicz, R.; Okada, T.; Jones, S. C.; Li, T.-D.; King, W. P.; Marder, S. R.; Riedo, E. High-Speed, Sub-15 Nm Feature Size Thermochemical Nanolithography. *Nano Lett.* **2007**, *7*, 1064–1069.

(47) Noel, S.; Liberelle, B.; Robitaille, L.; De Crescenzo, G. Quantification of Primary Amine Groups Available for Subsequent Biofunctionalization of Polymer Surfaces. *Bioconjugate Chem.* **2011**, *22*, 1690–1699.

(48) Palma, M.; Abramson, J. J.; Gorodetsky, A. A.; Penzo, E.; Gonzalez, R. L., Jr.; Sheetz, M. P.; Nuckolls, C.; Hone, J.; Wind, S. J. Selective Biomolecular Nanoarrays for Parallel Single-Molecule Investigations. *J. Am. Chem. Soc.* **2011**, *133*, 7656–7659.

(49) Schwartzman, M.; Palma, M.; Sable, J.; Abramson, J.; Hu, X.; Sheetz, M. P.; Wind, S. J. Nanolithographic Control of the Spatial Organization of Cellular Adhesion Receptors at the Single-Molecule Level. *Nano Lett.* **2011**, *11*, 1306–1312.

(50) Riedo, E.; Lévy, F.; Brune, H. Kinetics of Capillary Condensation in Nanoscopic Sliding Friction. *Phys. Rev. Lett.* **2002**, *88*, 185505.

(51) Yamamoto, Y.; Furuta, T.; Matsuo, J.; Kurata, T. Cleavage of Esters under Nearly Neutral Conditions at High Pressure. Chemo- and Regioselective Hydrolysis in Organic Solvents. *J. Org. Chem.* **1991**, *56*, 5737–5738.

(52) Carroll, K. M.; Desai, M.; Giordano, A. J.; Scrimgeour, J.; King, W. P.; Riedo, E.; Curtis, J. E. Speed Dependence of Thermochemical Nanolithography for Gray-Scale Patterning. *ChemPhysChem* **2014**, *15*, 2530–2535.

(53) Palaci, I.; Fedrigo, S.; Brune, H.; Klinke, C.; Chen, M.; Riedo, E. Radial Elasticity of Multiwalled Carbon Nanotubes. *Phys. Rev. Lett.* **2005**, *94*, 175502.

(54) Gao, Y.; Cao, T.; Cellini, F.; Berger, C.; De Heer, W. A.; Tosatti, E.; Riedo, E.; Bongiorno, A. Ultrahard Carbon Film from Epitaxial Two-Layer Graphene. *Nat. Nanotechnol.* **2018**, *13*, 133–138.

(55) Chinh, N. Q.; Gubicza, J.; Kovacs, Z.; Lendvai, J. Depth-Sensing Indentation Tests in Studying Plastic Instabilities. *J. Mater. Res.* **2004**, *19*, 31–45.

(56) Bhattacharya, A. K.; Nix, W. D. Analysis of Elastic and Plastic-Deformation Associated with Indentation Testing of Thin-Films on Substrates. *Int. J. Solids Struct.* **1988**, *24*, 1287–1298.

(57) Richeton, J.; Schlatter, G.; Vecchio, K.; Rémond, Y.; Ahzi, S. A Unified Model for Stiffness Modulus of Amorphous Polymers across Transition Temperatures and Strain Rates. *Polymer* **2005**, *46*, 8194–8201.

(58) Carroll, K. M.; Lu, X.; Kim, S.; Gao, Y.; Kim, H. J.; Somnath, S.; Polloni, L.; Sordan, R.; King, W. P.; Curtis, J. E.; Riedo, E. Parallelization of Thermochemical Nanolithography. *Nanoscale* **2014**, *6*, 1299–1304.

(59) Underwood, W. D. A Thin Film Polymer System for the Patterning of Amines through Thermochemical Nanolithography; Master Thesis; Georgia Institute of Technology, 2009.

(60) Dürig, U. Fundamentals of Micromechanical Thermoelectric Sensors. *J. Appl. Phys.* **2005**, *98*, No. 044906.

(61) Pires, D.; Hedrick, J. L.; De Silva, A.; Frommer, J.; Gotsmann, B.; Wolf, H.; Despont, M.; Duerig, U.; Knoll, A. W. Nanoscale Three-Dimensional Patterning of Molecular Resists by Scanning Probes. *Science* **2010**, *328*, 732–735.

(62) Gotsmann, B.; Lantz, M. A.; Knoll, A.; Dürig, U. Nanoscale Thermal and Mechanical Interactions Studies Using Heatable Probes. *Nanotechnology* **2010**, 121–169.

(63) Holzner, F. Thermal Scanning Probe Lithography Using Polyphthalaldehyde; Ph.D. Thesis; ETH Zurich, 2013.